REVIEW RESEARCH PAPER

Recent Development of Carbon Nanotubes Materials as Counter Electrode for Dye-Sensitized Solar Cells

M. Malekshahi Byranvand

School of Chemistry, University College of Science, University of Tehran, Tehran, Iran.

ABSTRACT

Dye-sensitized solar cells present promising low-cost alternatives to the conventional Silicon (Si)-based solar cells. The counter electrode generally consists of Pt deposited onto FTO plate. Since Pt is rare and expensive metal, nanostructured carbonaceous materials have been widely investigated as a promising alternative to replace it. Carbon nanotubes have shown significant properties such as cost-effectiveness, environmental friendliness, availability, corrosion resistance and excellent catalytic activity towards the redox species make them ideal for replacing Pt in the CEs of DSCs. The review presented below gives a succinct summary of the Carbon nanotubes materials in use as counter electrode in dye-sensitized solar cells .

INTRODUCTION

Climate change and the decreasing availability of fossil fuels require society to move towards more sustainable and renewable energy resources [1]. Solar energy is the source of nearly all energy on earth. Among all the renewable power sources, solar energy is the most easily exploitable, inexhaustible, quiet, and adjustable to enormous applications [2]. The solar energy incident on the earth's surface, whose globally convertible power is estimated to be 120,000 TW, is sufficient to satisfy the world's requirements [3]. Therefore, solar or photovoltaic (PV) technologies, which can harness solar energy, are of extreme importance. Solar PVs have the potential to offer a solution for declining energy reserves as well as the current climate change issues [4].

Historically, solar cell technologies have evolved into three generations [5]. First generation is a term that refers to the p-n junction PV, typically made from mono- and poly-crystalline silicon doped with other elements [6, 7]. However, these cells have high

✉ *Corresponding author
Email address: mahdi.malekshahi@gmail.com
Tel.: 98 916 9563283

fabrication cost and composition [8]. Thin film PV cells are the second generation of PV devices based on amorphous polycrystalline compound semiconductors. They are cheaper to produce, but the efficiency, which is less than 14% in amorphous thin film solar cells is lower than the efficiency exhibited by the single junction crystalline photovoltaic cell of the first generation that can reach as high as 27% [9]. The development of low-cost PV cells has been the topic of intensive research over the last three decades. The third generation PV cell technologies differ from first and second generation technologies by looking forward to optimize the efficiency and notably decrease costs [10]. Some examples of solar cells which fall under this category are dye-sensitized solar cells (DSCs) [11], quantum dot-sensitized solar cells (QDSSCs) [12], colloidal quantum dot solar cells (CQD) [13], organic solar cells [14], etc. The relation between the PV production cost per square meter with the solar cell module efficiency and the cost per unit power are shown in Fig. 1 [15].

Among the promising low-cost solar cells, DSCs, which can be fabricated using a non-vacuum printing

system, have attracted academic and industrial attention because of the demand for cost-effective, renewable energy sources [11, 16]. By far, the efficiency of DSCs sensitized by organometallic complex adsorbed on the semiconductor nanocrystalline TiO_2 and Cobalt (II/III)–based redox electrolyte has reached 13% [17].

However, there are a number of challenges facing further development of DSC technology, mostly associated with the leakage of liquid electrolytes, degradation of the dyes, increasing demands for new transparent electrode materials and need to a precious metal such as Pt for counter electrode (CE). Pt has been extensively used in the CE of DSCs due to its high electro-catalytic nature and high conductivity [18, 19]. However, platinum is an expensive and a rare material that contributes significantly to the overall cost of DSCs [19, 20]. Due to concerns of the high cost of platinum, different type carbonaceous materials have been investigated as potential low cost replacements for platinum [21, 22]. Among these compounds, CNTs have shown significant properties such as cost-effectiveness, environmental friendliness, availability, corrosion resistance and excellent catalytic activity towards the redox species make them ideal for replacing Pt in the CEs of DSCs [23, 24]. In this review, recent advances in CNTs and their application as counter electrode for DSCs are discussed.
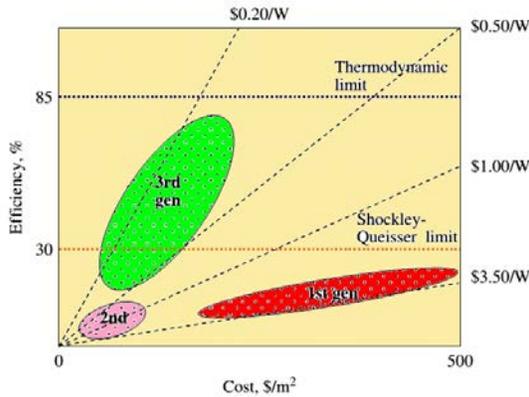
Fig. 1. Efficiency-cost trade-off for the three generations of solar cell technology, wafers, thin-films and advanced thin-films (year 2003 dollars)[15].

STRUCTURE AND OPERATION PRINCIPLE OF DSCS

A schematic representation of operating principles of typical DSC is illustrated in Fig. 2. [25].

In DSCs, light is harvested by dye molecules grafted on a large surface and wide band gap semiconductor (such as TiO_2) in contact with an electrolyte containing a redox pair as a charge mediator (I^-/I_3^-), while the circuit is closed by a counter electrode, usually made of Pt [26]. Via absorption of a photon (excitation) by dye molecules, electron changes from the electronic ground state (HOMO) to the excited state (LUMO) [27]. The excitation of the dye upon irradiation is followed by injection of the resulting electrons into the conduction band (CB) of the semiconductor, from where they reach the cell anode [27, 28]. Regeneration of dye electrons occurs through electron donation from a redox electrolyte in contact with the dye [29]. Triiodide is reduced in turn at the counter electrode, while electron migration from the anode to the cathode (counter electrode) closes the circuit [30]. The voltage generated is equal to the difference between the Fermi level of the electron in the solid TiO2 and the redox potential of the electrolyte [31].
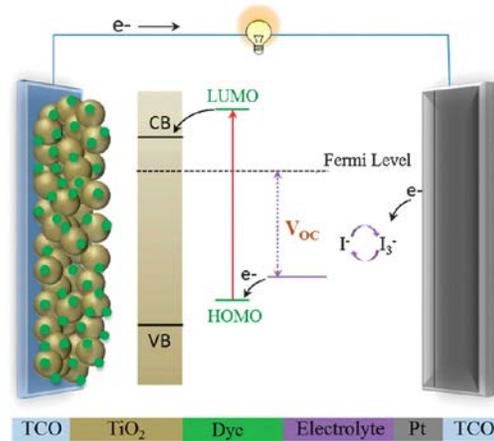
Fig. 2. Schematic representation of the composition and the operating principle of a DSC [25].

The solar energy-to-electricity conversion efficiency (η) of DSCs can be defined by the following conversion efficiency formula (Eq. 1) [32, 33]:

$$\eta = \frac{Pmax}{Pin} \tag{1}$$

Where, Pmax is the maximum output power and Pin is the input power (incident light) measured in $mWcm^{-2}$. The fill factor (FF) of the DSC is a measure of series resistance and junction quality of the cell, which can be defined using as follows (Eq. 2):

$$FF = \frac{Pmax}{Isc \times Voc} \qquad (2)$$

Where Jsc and Voc are the short circuit currents (measured in mAcm^{-2}) and the open circuit voltage, respectively.

NANOCARBON MATERIALS

Nanocarbon is a term increasingly used to indicate the broad range of carbon materials having a tailored nanoscale dimension and functional properties that significantly depend on their nanoscale features [34, 35]. The alternative definition (also often used) is nanostructured carbon. CNT and graphene belong to this class of materials comprising many more types of carbon materials, such as nanofibers, -coils, -diamonds, -horns, -onions, and fullerene [36]. The nanocarbon class of materials is typically extended to include carbon nanocomposites with metal ions, metal oxide, metals, and quantum dots used in various applications [37, 38] as advanced electrodes for energy conversion and storage, as well as other applications such as catalysis. These carbon/inorganic nanohybrids are at the frontier of research for the development of advanced devices for sustainable energy and development, [39] including artificial leaves [40].

The field of application of nanocarbon materials is large, because they possess electrical and thermal conductivity, as well as a mechanical strength and lightness that conventional materials cannot match [41]. For these reasons, they are extensively studied in applications going from photonics and optoelectronics to biotech and nanomedicine, advanced electrodes, and polymer composites [1]. Fig. 3 provides a schematic illustration of some nanocarbons. However, carbon nanomaterials display remarkable electrical, thermal, and mechanical properties that enable several exciting applications in DSCs.

CARBON NANOTUBES (CNTS)

CNTs were discovered accidently by Sujimo Iijima in 1991 [42]. While making buckyballs, Iijima noticed long, needlelike structures (the CNTs) mixed in with the buckyballs. CNTs are also classified as single-walled carbon nanotubes (SWCNTs) or multi-walled carbon nanotubes (MWCNTs) [43]. Typical diameters for SWCNTs and MWCNTs are 0.8–2 nm and 5–20 nm, respectively. Length of nanotubes can vary from less than 100 nm to few centimeters [44].

Although SWCNTs are potentially preferable for a number of applications (surface area, for example, may be
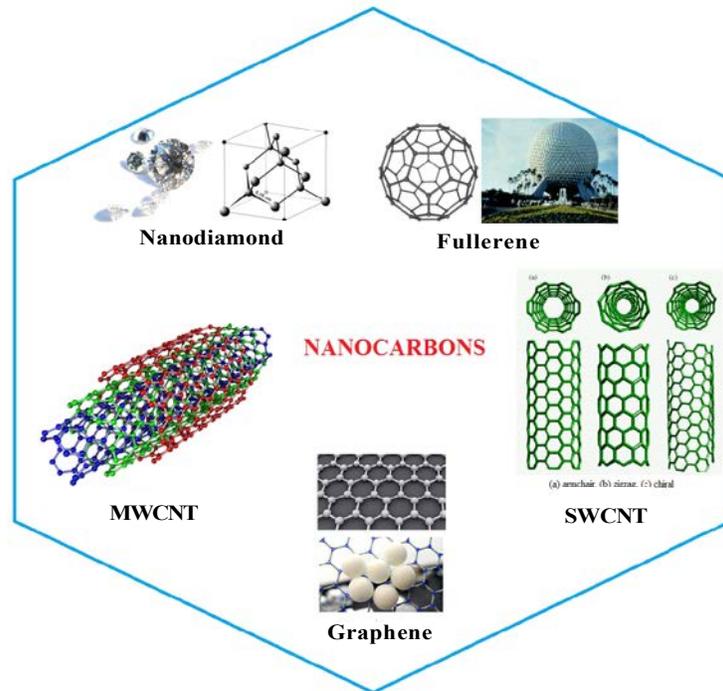
Fig. 3. Schematic illustration of some nanocarbon

5 times higher than that of MWCNTs), the lack of mass production (at a reasonable cost) is still a limit for their practical use [45]. SWCNTs resemble a single graphene sheet rolled up, while MWNT are made up of several SWCNTs nested inside each other [46-48]. There are three types of nanotubes: armchair, zig-zag and chiral (see Fig. 3). The three forms are characterized by the orientation of the hexagonal patterns within the graphene sheets. Though the structural differences in the three types of CNTs are subtle, they give rise to very different properties [49]. The electrical property of CNTs materials depends a lot on the structure of the nanotubes [50]. For example, chiral and zigzag CNTs can be semiconductors. Armchair and some zigzag CNTs are metallic conductors. Metallic CNTs conduct electricity better than copper because of the way that electrons travel through the CNT. Since the CNT is hollow tube, the electrons are confined and travel only along the surface of the tube. Since the electrons have fewer directions to move in, they are able to travel along the CNT and lose a minimal amount of energy. In a copper wire, the electrons have three dimensions they can travel in. This extra dimension increases the amount

Fig. 4. Optical photography of the catalyst before (a) and after (b) the reaction, showing the remarkable increase in volume during CNT growth. The MWCNT yield is 179 gCNT·gcatalyst"1. (c) SEM image of the MWCNTs and their external diameter distribution (inset) [62].

of scattering possible, and so electrons lose energy from colliding with copper atoms [51].

Most importantly, CNT-based heterojunctions are of particular interest because of their unique geometry as well as excellent electronic, thermal and mechanical properties [52]. Free electron/hole pairs excited by photons can be either separated by an externally applied voltage [53], by internal fields at the Schottky barriers [54], at p–n junctions [55] or at defects [56]. A photocurrent [57] or a photovoltage [57] can be generated. The photocurrent in CNT junctions shows band-to-band transitions and photon assisted tunneling with multiple sharp peaks in the infrared, visible and ultraviolet. Besides individual CNT, CNT macro-bundles [58] and films [59] also produce a photocurrent.

High temperature preparation techniques such as Arc discharge or laser ablation were first used to produce CNTs but nowadays these methods have been replaced by low temperature chemical vapor deposition (CVD) techniques (<800 °C), since the orientation, alignment, nanotube length, diameter, purity and density of CNTs can be precisely controlled in the latter [60]. The most utilized methods and some of other non-standard techniques like liquid pyrolysis and bottom-up organic approach are used to CNTs synthesis. Most of these methods require supporting gases and vacuum, but the growth at atmospheric pressure has been already reported [61]. However, gas-phase methods are volumetric and hence they are suitable for applications such as composite materials that require large quantities of nanotubes and industrial-scale synthesis methods to make them economically feasible.

CVD is the only method to scale-up the production of multiwalled CNTs. Tessonnier et al. [62] showed that in an optimized CVD process, 1 g of spinel-type cobalt-manganese-based mixed oxide catalyst can produce about 180 g of MWCNTs, when exposed to an ethylene/hydrogen feed at 650 °C for 2 h (Fig. 4).

CNTs MATERIALS AS COUNTER ELECTRODE FOR DSCS

For a low-cost DSC, we have to consider a cheap and abundant material in the earth's crust as the material for application in DSCs. However, carbon which is the sixth most abundant material in the earth's crust is the best material to replace in different parts of DSCs. Mainly due to its core features like cost-effectiveness, environmental friendliness, availability,
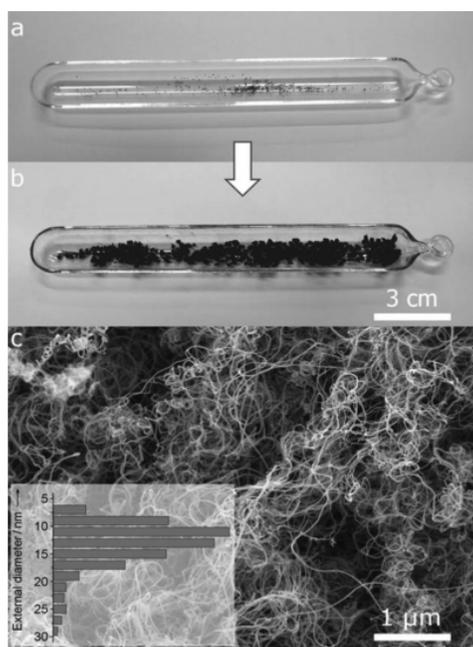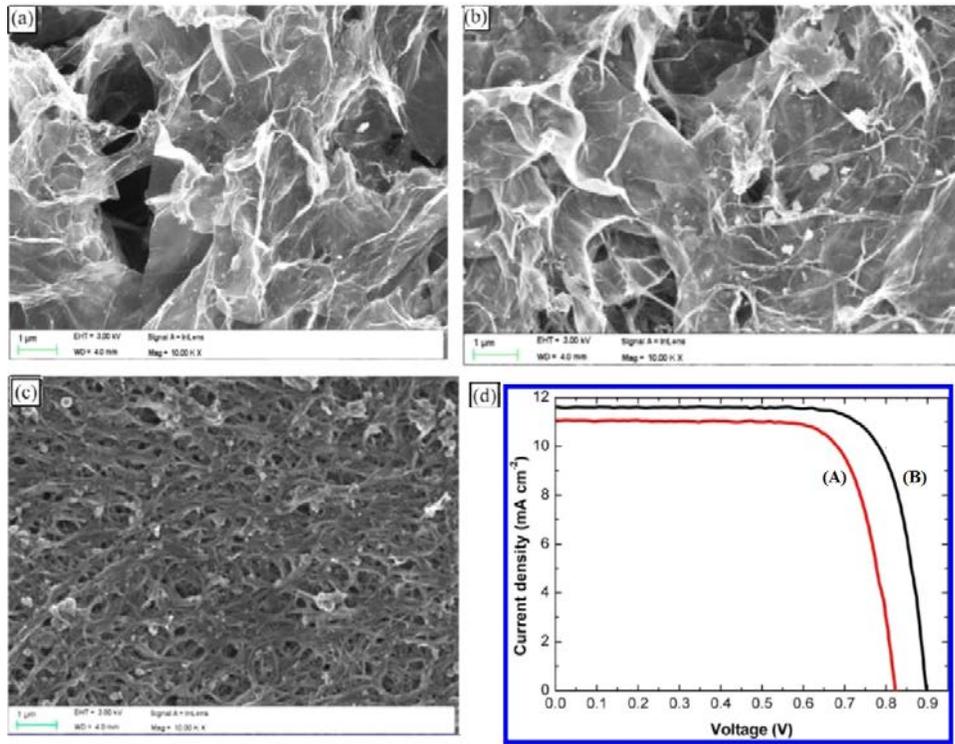
Fig. 5. SEM images of (a) rGO, (b) rGS-20, (c) SWCNTs, (d) J-V curves of DSCs with (A) Pt and (B) rGS-20 as the counter electrode after 7 days [79].

corrosion resistance and excellent catalytic activity towards the redox species, carbon is an attractive option [63, 64].

Even though Pt is the best preferred material for DSC, it also possess some disadvantages like high cost (~$1456.55 per Troy Oz at present), low abundance of material, diminishing catalytic property on exposure to dye solution, and stability due to the corrosive nature of the electrolyte [65, 66]. These reasons open up a new way for the invention of other conducting material for the counter electrode like CNTs [67-71].

The utilization of CNTs in counter electrodes has attracted a great interest as a replacement for highly expensive platinum and due to their activity for I3" reduction, electronic conductivity, and easy availability [72]. The variety of CNTs also allows for tuning important features such as electrode thickness, surface area and porosity [73-75]. There are several reports on the use of CNTs as counter electrodes in DSCs [1, 44, 72, 76, 77].

SWCNTs have a high longitudinal conductivity. Suzuki et al. used of SWCNTs for the CE [78], which were deposited on both FTO-glass and a Teflon membrane filter achieving conversion efficiencies of 3.5% and 4.5%, respectively. SWCNTs are good triiodide reduction catalysts. In addition, the sheet resistance of the SWCNTs on the Teflon membrane (1.8 Ω cm-2) is four times lower than that of FTO-glass (ca. 8-15 Ωcm-2) rendering them an attractive choice for large-area DSC modules.

To increase the Voc of DSCs, it is crucial to enhance the photovoltaic efficiency of DSCs. Zheng and coworkers reported an effective method to significantly improve the Voc and photovoltaic efficiency of DSCs by using gel-coated composites of reduced graphene oxide (rGO) and SWCNTs as the counter electrode (Fig. 5a-c) [79]. The Voc and power conversion efficiency (PCE) were 0.86 V and 8.37% for fresh DSCs with the composite of 80 wt % rGO and 20 wt % SWCNTs (rGS-20), significantly higher than those (Voc= 0.77 V, PCE = 7.79%) of control DSCs with Pt fabricated by pyrolysis as the counter electrode. The Voc value of DSCs with rGS-20 as the counter electrode further increases to 0.90 V after one week (fig. 5d). The high Voc and PCE were
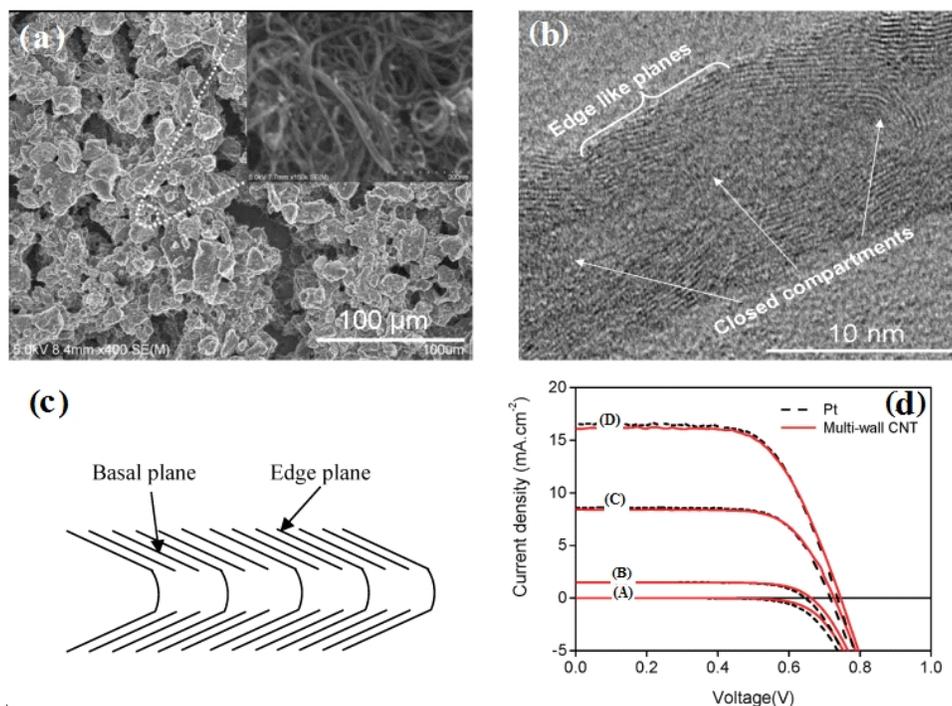
Fig. 6. Microstructural characterization of multiwall CNTs: (a) FE-SEM image of a multiwall CNT/CMC composite film on a fluorine-doped SnO2-conducting glass substrate. Inset: enlarged view of the marked portion. (b) TEM image of the bamboolike structure in multiwall CNTs used in this study. (c) Schematic of the bamboolike-structure multiwall CNT. (d) J-V characteristics of DSSC with multiwall CNT (solid line) and platinum (dashed line) counter electrodes. Curve (A) shows the performance of devices in the dark. Curves (B-D) were measured under 0.1, 0.5, and 1 sun illumination (air mass 1.5 G), respectively [21].

ascribed to the synergetic effects of rGO and SWCNTs in reducing the over potential of the I3" reduction. The rGO with high specific surface area can have high electrocatalytic activity, whereas SWCNTs give rise to high conductivity for the composites and facilitate the penetration of the redox species into rGO sheets by preventing the agglomeration of the rGO sheets.

Also, Lee et al. used the bamboolike-structure MWCNT as counter electrodes for I3- reduction in DSCs (Fig. 6a, b) [21]. Through taking advantage of the defect-rich edge planes along the tube fast electron kinetics at the electrode-electrolyte interface could be facilitated. Results showed that a CE based upon these bamboolike tubes was comparable to that obtained when a Pt CE was employed. The catalytic performance of the CE was examined through the rate of charge transfer (RCT) across the CE. Values for this electrode dropped from 1.8 Ùcm"2 (Pt) to 0.82 Ùcm"2. The reasons for such high catalytic activity has been attributed to the high surface area of the CE and the defect-rich basal plane, it has also been debated that this may also

be attributed to residual catalyst particles located in the nanotubes (Fig. 6 c). Overall the device performed well and achieved an efficiency of 7.67% which compared to 7.83% for the Pt based cell (Fig. 6 d).

CNT/polymer composite as CE for DSCs

In CNT/polymer composite materials, advantages including high surface area, excellent electrical and electrocatalytic properties, and high stability from CNTs with good flexibility, abundant supply, and easy fabrication from polymers are combined [68, 80]. In the current composite electrodes, however, CNTs are typically interconnected to form networks, and the generated charges have to hop through a lot of boundaries among CNTs. He et al. were synthesized polyaniline-single wall nanotube (PANi-SWCNT) complexes using a reflux technique which are employed as counter electrodes (CEs) for DSCs (Fig. 7a, b) [68]. Owing to the facile charge transfer between PANi (N atoms) and SWNT (C atoms) by a covalent bond (Fig. 7c), electrical conduction, electrocatalysis, and therefore conversion efficiency have
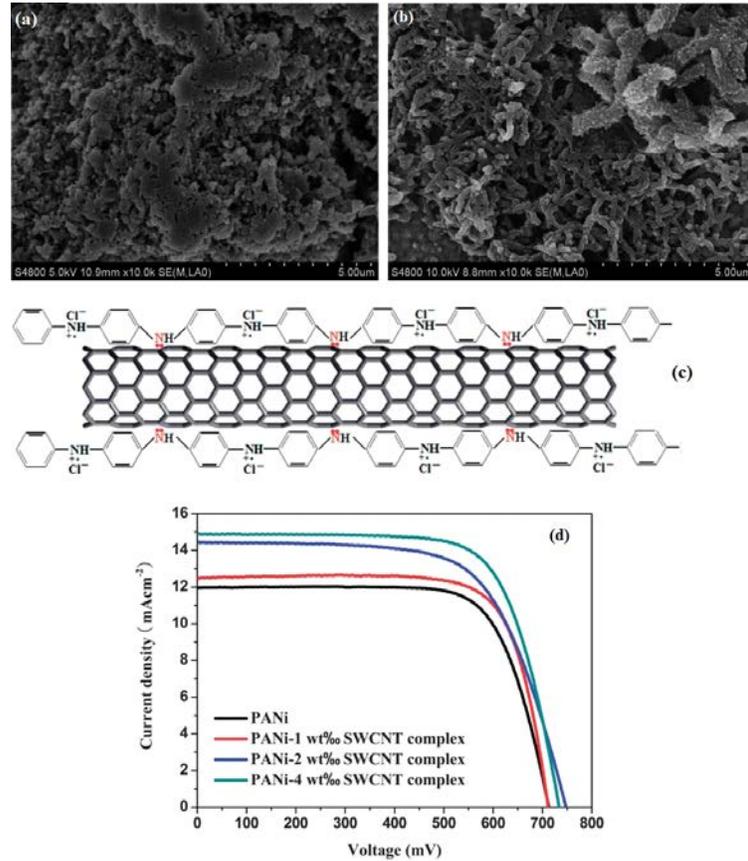
Fig. 7. SEM photographs of (a) PANi and (b) PANi-4wt%SWCNT complex CEs. (c) proposed complexation mechanism between PANi and SWCNT. (d) J–V characteristics of DSSCs from pure PANi and PANi-SWCNT complex CEs [68].

been markedly elevated in comparison with that of PANi-only CE. The DSC employed PANi-4%wt SWCNT complex CE gives an impressive power conversion efficiency of 7.81% (Fig. 7d). The high conversion efficiency, facile charge-transfer in combination with simple preparation, relatively low cost and scalability demonstrates the potential use of PANi–SWCNT complex in robust DSCs.

Yang group developed a perpendicularly aligned and penetrated CNT/polymer composite film through a simple slicing technique (Fig. 8 a-f) [80]. This novel composite film exhibits good transparency, high flexibility, excellent electrical conductivity, and remarkable electrocatalytic activity, and may be widely used for various electrode materials. As a demonstration, DSCs using these composite films ranging from 10 to 40 μm in thickness were fabricated and tested under AM 1.5 illumination. As a comparison, the cell derived from the composite film with thickness of 10 ìm without optimization showed slightly decreased V_{OC} and FF but increased J_{SC} under the same conditions.

Core-shell structures of CNTs and polymers are also used as CE material in DSCs. Shin et al. [81] synthesized highly conductive and thermally stable CNT/PEDOT core/shell nanostructures by a modified emulsion polymerization technique (Fig. 9). CNT/PEDOT core-shell structures as counter electrode in DSCs showed an efficiency of 4.62% with a high fill-factor. Moreover, the core-shell nanostructures exhibited higher thermal stability and electrical conductivity compared to pure PEDOT [82, 83].

Aligned carbon nanotube-oriented PEDOT:PSS composites show an unexpectedly high catalytic activity which greatly exceeds the aligned individual components, the non-aligned composite counterpart, and even conventional platinum. When they are used
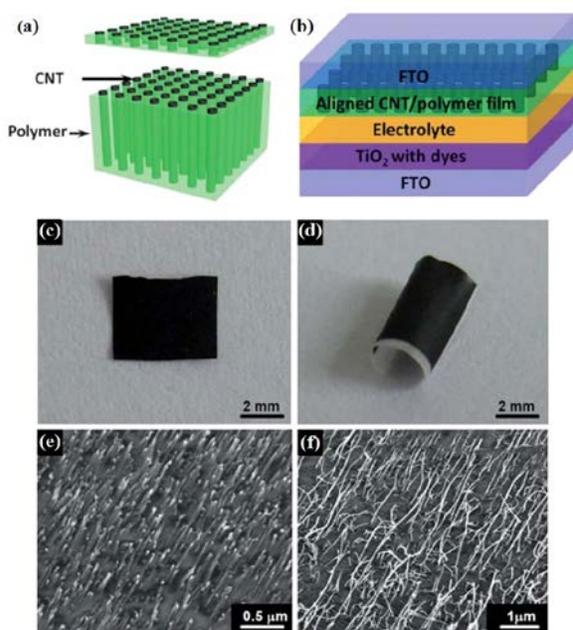
Fig. 8. (a) A schematic illustration of fabrication of the perpendicularly aligned and penetrated CNT/polymer composite film as a counter electrode. (b) The structure of a DSC using the composite film as a counter electrode. (c, d) Photographs of a composite film with different morphologies. (e) SEM image from a top view, (f) SEM image from a side view [80].
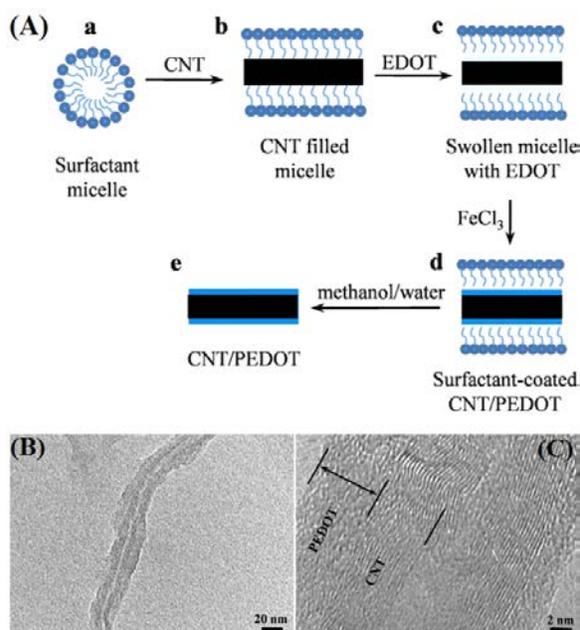
Fig . 9. (A) Schematic illustration for the synthesis of CNT/PEDOT core/shell nanostructures.(B, C) TEM images of the CNT/PEDOT nanostructures [81].

as counter electrodes in dye-sensitized solar cells, the aligned composites also exhibit a highest energy conversion efficiency of 8.3% [84]. The synergetic ï-ï interaction between the nanotubes and polymers by aligned organization is the key to this new phenomenon (Fig. 10).

Also, by Yun et al. the dispersion of MWCNT in PEDOT:PSS solution was studied and various concentrations of MWCNT/PEDOT:PSS solution were evaluated [85]. The MWCNT/PEDOT:PSS composite films showed much lower sheet resistance in the range of 730-2150 $\Omega.cm2$, and higher surface roughness in the range of 25-110 nm than the pure PEDOT:PSS film (980 k $\Omega.cm2$, and 0.82 nm) depending on the MWCNT content in the composite. The high conductivity and roughness of MWCNT/PEDOT:PSS films enhanced its performance as a catalytic counter electrode in the DSC.

Metallic/CNT composite as CE for DSCs

Metallic/CNT composites have recently been shown to have extremely promising results for CE applications in DSCs.

Liu et al [86] reported a solvothermal technique for obtaining a CE with a composite film of Pt/CNT. The film was used directly as the counter electrode (CE) in a DSC, which exhibited a Jsc of 16.6±0.2 mA cm-2 and a η of 6.96±0.09% at 100 mWcm-2 illumination. The CE in this case shows both high electric conductivity and high roughness, and thereby an extraordinary catalytic ability for the reduction of triiodide ions. These results are comparable with DSCs based on conventional Pt-CE, and feasible for replacing the conventional transparent conductive oxide (TCO) conductive layer in DSCs. Taking advantage of the high surface area of MWCNTs and the catalytic properties of both Pt and MWCNTs has led to the development of MWCNT–Pt composite materials for DSSCs by Ho et al [87]. Pt nanoparticles dispersed on MWCNTs were shown to have ç of 8.00±0.23% compared to ç of 6.92±0.07% for the Pt cell. The enhancement in the efficiency of these devices is attributed to the higher Jsc value obtained which increased from 14.62±0.19 to 18.01±0.91 mA cm⁻² (Fig. 11). From examination of the surface morphologies it was concluded that the Pt-MWCNT CE had a rougher surface and hence a higher catalytic activity than that of the Pt CE.

Guo group newly were developed a novel strategy to prepare hybrid nanomaterials of platinum nanoparticles and multi walled carbon nanotubes (Pt–MWCNTs) (Fig. 12a) [73]. A thin layer of sulfur on
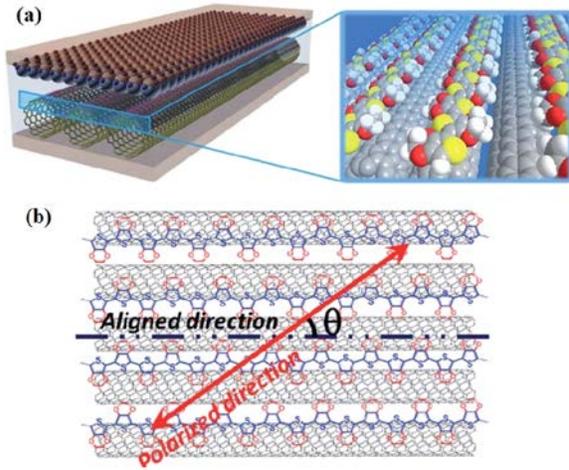
Fig. 10. (a) Schematic illustration of the oriented PEDOT:PSS on aligned CNTs for efficient DSCs. The grey, white, yellow and red colors correspond to elements C, H, S and O, respectively. (b) Schematic illustration of the included angle (θ) between the polarized and CNT-aligned directions [84].

Fig. 11. I-V characteristics of DSCs with Pt CE and Pt-MWCNT CE measured at 100 mW cm"2 and in the dark. The insert is the IPCE curves for the corresponding devices [87].

MWCNTs absorbed and binds the Pt precursors from solution on the MWCNTs' surface and also restricts their particle growth during reduction which resulted in ultrafine dispersions of metal nanocrystalline due to the strong affinity of sulfur for noble metals. The morphology and elemental composition of Pt–MWCNTs were characterized by SEM, TEM and EDS (Fig. 12b-e). The composite material was applied as the counter electrode (Pt–MWCNTs CE) for DSCs and the FF and ç of the DSC with Pt–MWCNTs CE were 0.63 and 7.69%, respectively. The corresponding values of the DSC with bare Pt CE were 0.55 and 6.31%.

A free radical assisted strategy was introduced into the functionalization of counter electrode materials for the first time by Yang et al [24]. They were claimed that, with the assistance of a radical initiator, short-chained thiol groups can be attached on a multi-walled carbon nanotube (MWCNT) surface covalently, which was confirmed to be beneficial for both controlling the particle growth of platinum (Pt) on MWCNTs and improving the electron transfer between counter electrode materials and the substrate (Fig. 13a, b). The obtained Pt-MWCNT composite has been applied as a counter electrode material for DSCs, and the ç was detected to be 8.62%, surpassing that of the cell with a conventional Pt counter electrode (η=7.56%) (Fig. 13c).

Recently, some inorganic compounds have also been introduced into DSCs as electrocatalysts, such as nitrides [88, 89], sulfides [90, 91], selenides [92], and carbides[93, 94], which show good catalytic activity as CE materials.

Lin et al. were successfully synthesized One-dimensional (1D) hierarchical nanostructures composed of CoS1.097 nanoclusters directly grown on CNT backbone (CNT@CoS1.097) by a facile glucose-assisted hydrothermal method (Fig. 14a-f) [95]. It was found that glucose acted as a binder to assist the hierarchical CoS1.097 nanoclusters grown on the surfaces of CNTs with uniform coverage along the longitudinal axis. The extensive electrochemical measurements confirmed that the CNT@CoS1.097 nanocomposite indeed provided simultaneously enhanced electrical conductivity and superior electrochemical activity as electrode materials for DSCs and supercapacitors (SCs). The DSC assembled with the CNT@CoS1.097 nanocomposite counter electrode (CE) achieved an enhanced photovoltaic conversion of 7.18% to those of DSCs based on the Pt, CNT, and CoS1.097 CEs (Fig. 14g-i).

The use of MWCNT webs as a CE was investigated by Noureldine et al.[96]. The CE was made of 20 layers of MWCNT webs surpassed CoS and Pt as electrocatalytic materials on FTO (Fig. 15 a, b). The good performance (η=4.12%) of these webs was attributed to their better electroactivity towards the regeneration of the electrolyte system at the cathode (Fig. 15 c, d).

Yue group were synthesized multi-wall carbon nanotubes decorated with tungsten sulfide (MWCNTs-WS2) by using a hydrothermal method, and used as a
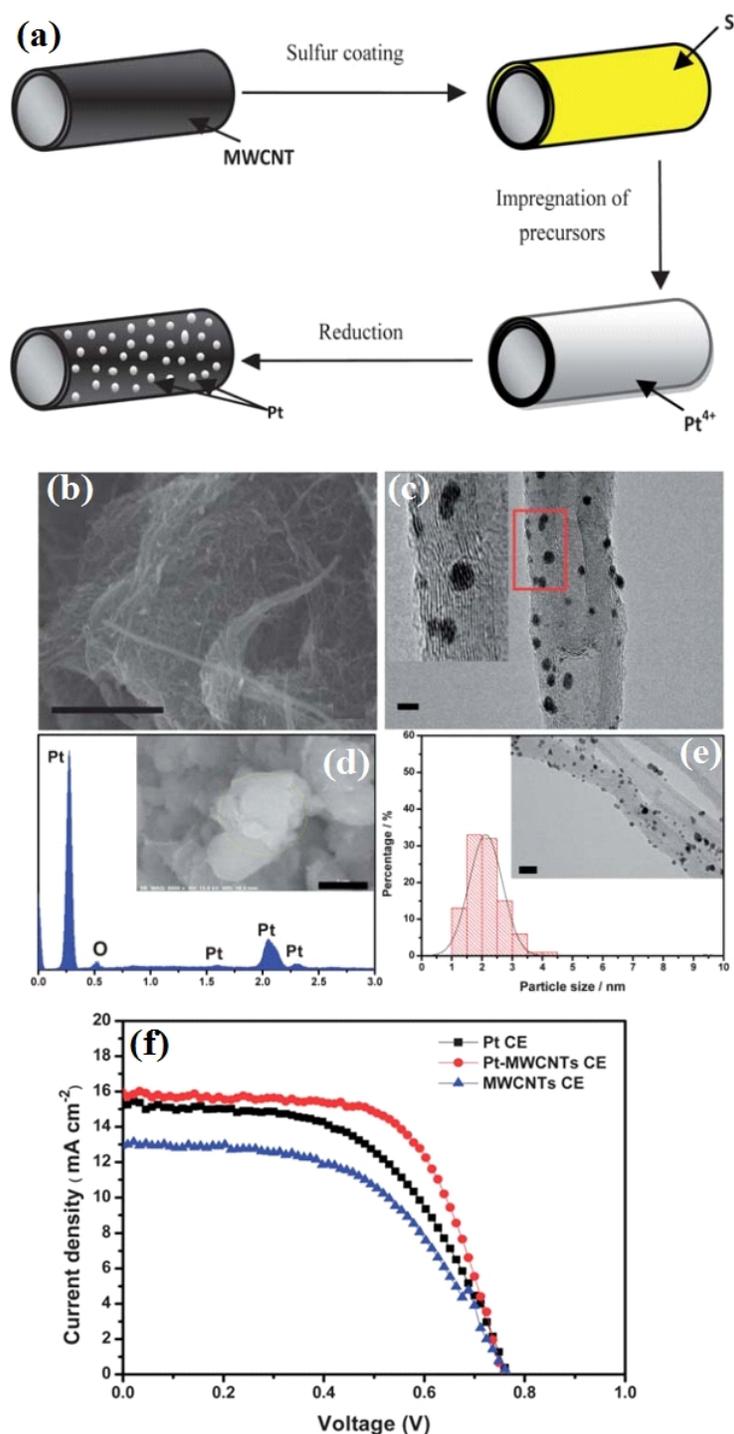
Fig. 12. (a) Schematic illustrating the nucleated-growth synthesis of MWCNT-supported Pt. (b) SEM image of Pt-loading MWCNT (scale bars: 1mm). (d) EDS spectrum of Pt–MWCNTs (inset SEM with scale bar: 3mm). (c) TEM image of monodispersed Pt nanoparticles on MWCNTs (scale bar: 5 nm) and (e) nanocrystallite size distribution of Pt nanoparticles loaded on MWCNTs (based on a count of 100 crystallites, inset TEM with scale bar: 10 nm). (f) J-V of the DSCs with Pt CE, Pt–MWCNTs CE and MWCNTs CE [73].

(a)

(b)

(c)
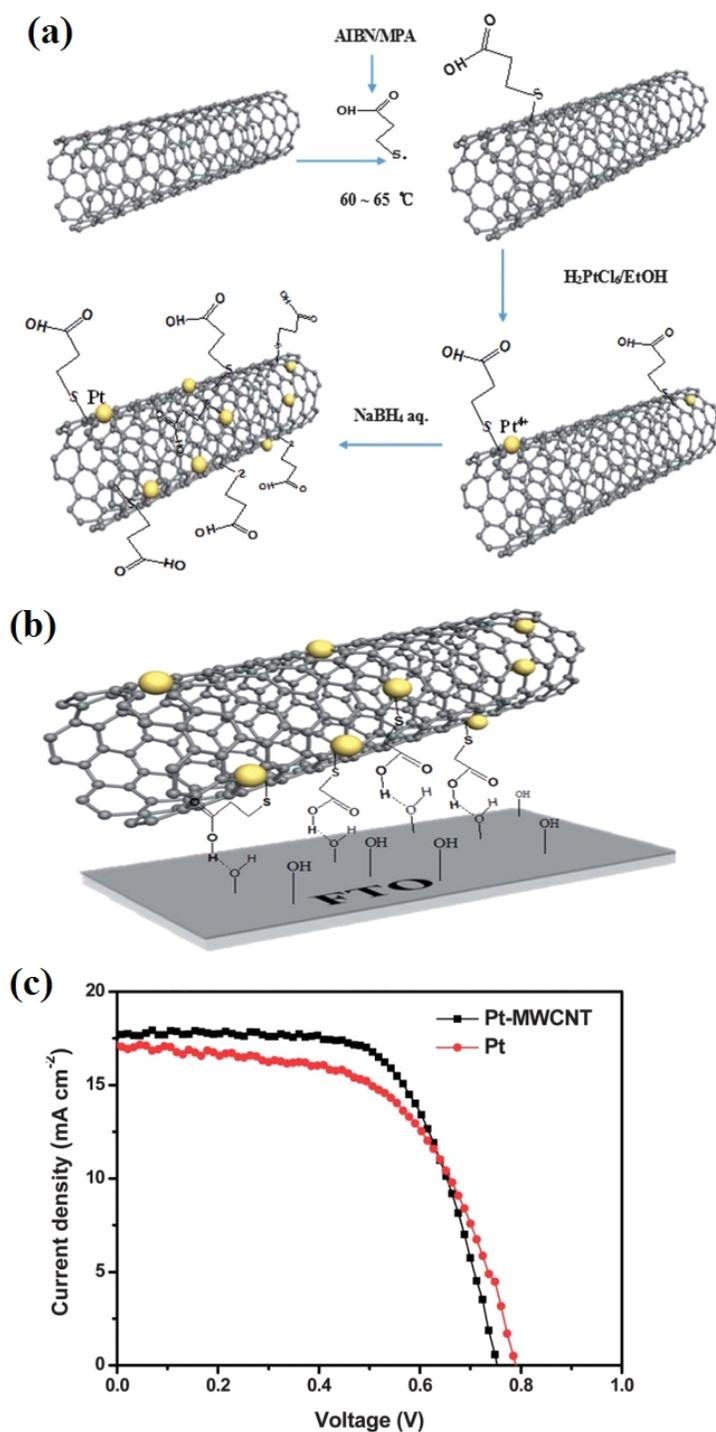
Fig. 13. (a) Schematic diagrams of the synthesis of the Pt–MWCNT composite, including the radical reaction process and the loading of platinum over the carbon surface defects. (b) Schematic illustrating the interaction between the carboxyl groups exposed outside the MWCNT surface with the hydroxyl groups on the FTO surface. (c) Photocurrent density–voltage characteristics of DSCs with different CEs [24].
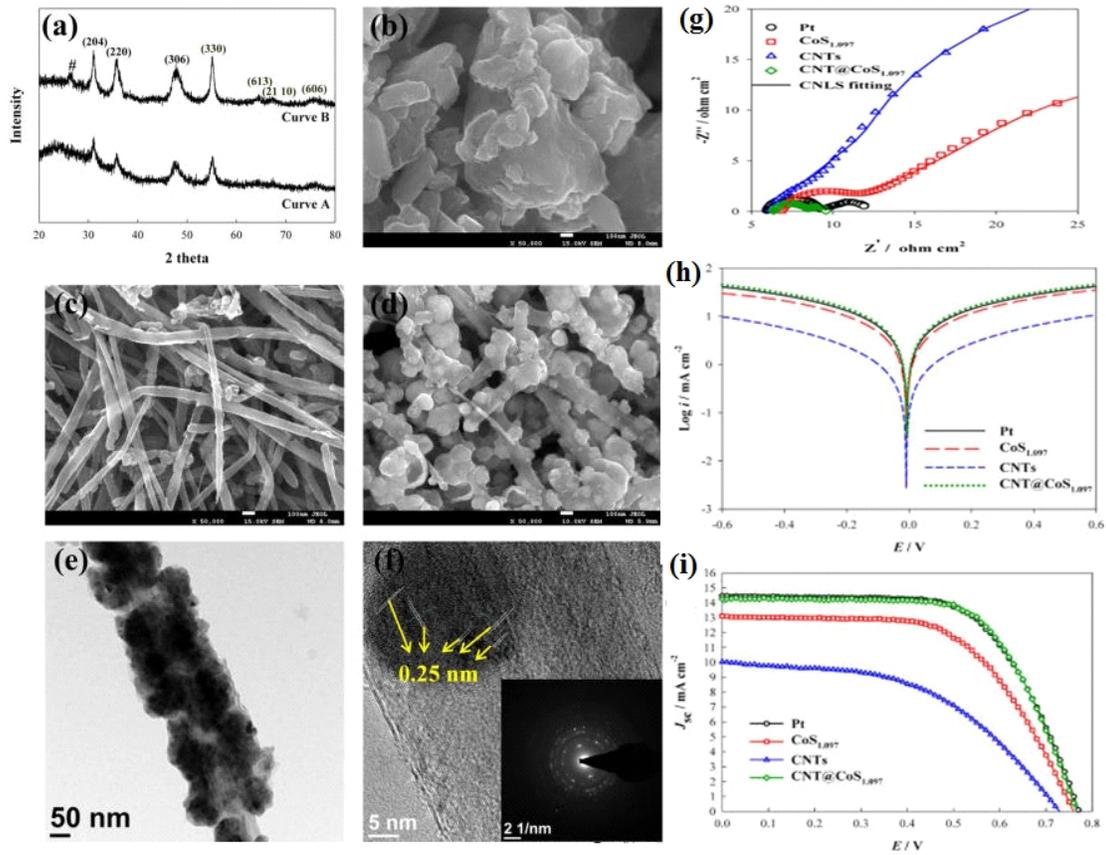
Fig. 14. (a) XRD patterns of CoS1.097 (curve A) and CNT@CoS1.097 (curve B). (b"d) FESEM images of CoS1.097, CNTs, and CNT@CoS1.097, respectively. (e"f) TEM and HRTEM images of CNT@CoS1.097. (g, h) Nyquist plots and Tafel polarization curves of the symmetric cells composed of two identical CEs. (i) Photovoltaic characteristics of the DSCs assembled with different CEs [95].
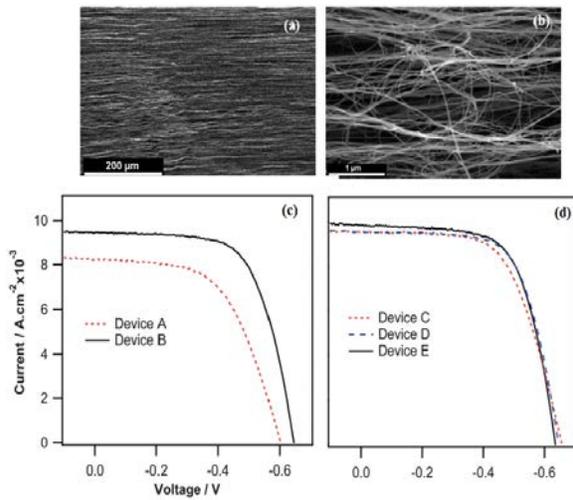
Fig. 15. SEM image of MWCNT web (a) Magnification 100 o and (b) 20 000 o. (c) J–V curves of device A with Pt CE (dotted) and device B with CoS CE (solid). (d) J-V curves of device C with 5 layers (dotted), device D with 10 layers (dashed) and device
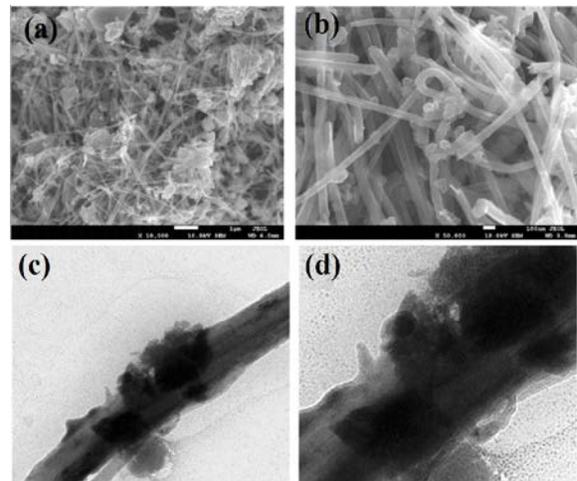
Fig. 16. SEM (a, b) and TEM (c, d) images of MWCNTs-WS$_2$ [97].

12
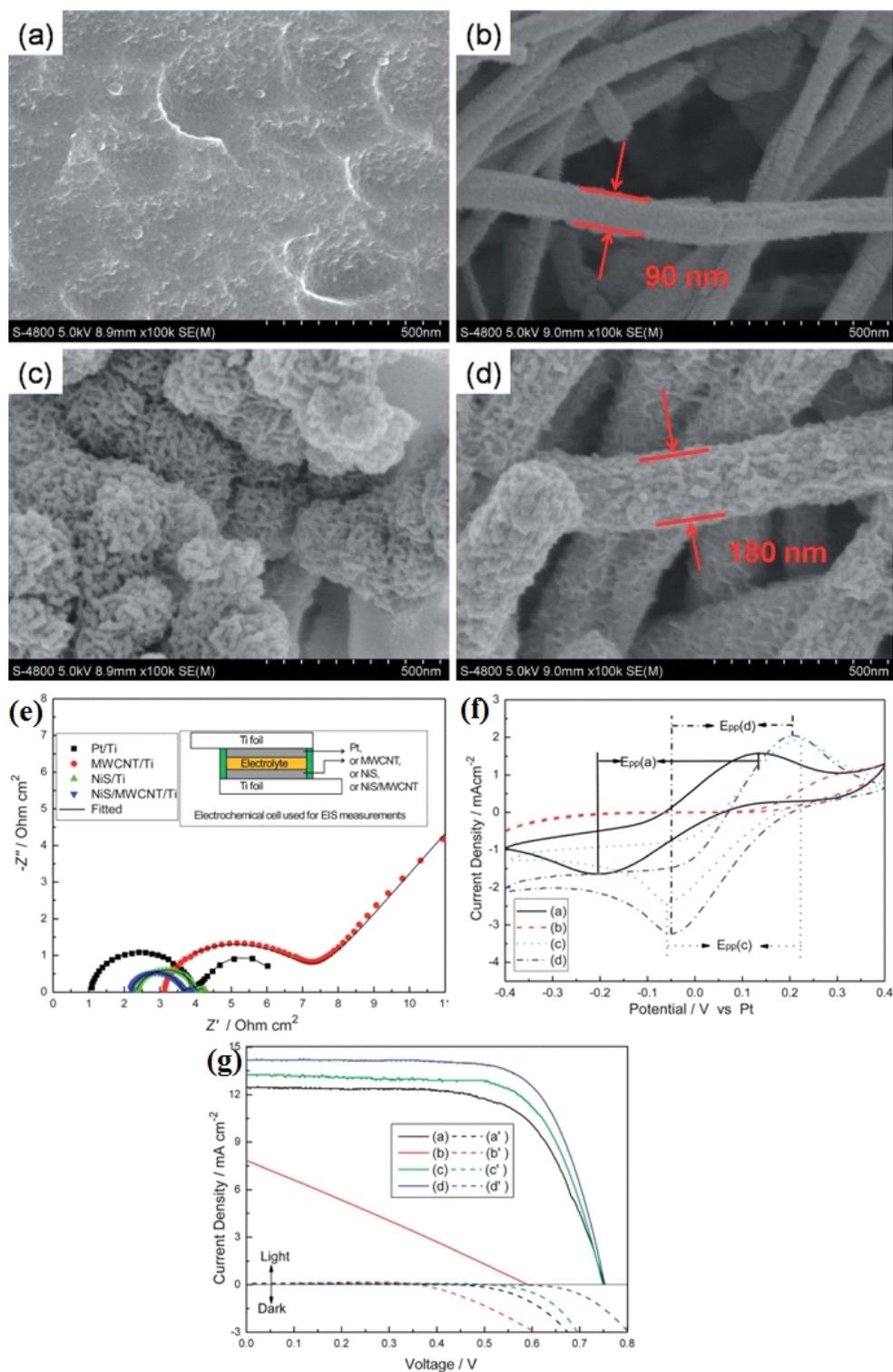
Fig. 17. FESEM images of Ti (a), MWCNT/Ti (b), NiS/Ti (c), and NiS/MWCNT/Ti (d) CEs, respectively. Nyquist plots and CVs of the different CEs (e, f), Photocurrent–voltage curves of the DSSCs based on different CEs (g) [98].

low-cost platinum-free counter electrode for DSC [97]. Fig. 16a-d shows SEM and TEM images of MWCNTs-WS2. The combination of WS2 with MWCNTs increased the electrocatalytic activity due to the large specific area and high conductivity of MWCNTs. A DSC based on this counter electrode achieved a high power conversion efficiency of 6.41%. This efficiency is comparable to 6.56% for a DSC with Pt counter electrode.

The high performance NiS/MWCNT/Ti hybrid film was firstly used as a Pt free CE in DSCs by Xiao et al. [98]. In this work, MWCNTs were deposited on a Ti foil substrate by using electrophoresis, then, a NiS layer was deposited on the MWCNTs by using a pulse potentiostatic method. The resultant MWCNTs were uniformly wrapped with a nano-corallines NiS thin film in the thickness of about 45 nm (Fig .17a-d). The characterization of CVs and EIS indicated that nano-corallines NiS had high electrocatalytic activity for I3-reduction (Fig .17e, f). Under full sunlight illumination, the DSCs based on the NiS/MWCNT/Ti CE achieved a light-to-electric energy conversion efficiency of 7.90%, which was higher than the DSCs based on the Pt/Ti CE (6.39%) (Fig. 17g).

CONCLUSION

The efficiency of DSCs is approaching the efficiency level needed for commercialization. However, Pt is an expensive noble metal and for the worldwide commercialization of DSCs, this needs to be replaced with inexpensive materials. Mainly due to its core features like cost-effectiveness, environmental friendliness, availability, corrosion resistance and excellent catalytic activity towards the redox species, CNTs is an attractive option. It has been clearly demonstrated that different types of CNTs and their various combinations such as metallic/CNT and CNT/polymer were used as CE materials. In this work, electrochemical properties of various types of CNs materials as CEs and their effects on DSCs performance were reviewed. Further, the role of functional groups on electrocatalytic behavior of CNTs CEs was presented.

Though tremendous amount of work has been done to optimize various aspects of CNTs materials as counter electrode, most of the reported DSC performance is still lower when compared to Pt CEs. Further improvement in DSCs performance using CNTs CEs requires morphologies with higher surface area and higher conductivity. Dimensions such as nanostructure diameter and length can be optimized

for maximizing conductivity and surface area. Surface defects can be optimized so as to enhance catalytic activity without significantly reducing conductivity. For composite structures employing platinum, loading of platinum should be minimized to minimize cost. Also, more accurate electrical models should be developed to better understand and minimize various internal resistances.

CONFLICT OF INTEREST

The authors declare that there are no conflicts of interest regarding the publication of this manuscript.

REFERENCES

[1] L.J. Brennan, M.T. Byrne, M. Bari, Y.K. Gun'ko, Advanced Energy Materials, 1 (2011) 472-485.

[2] N.A. Ludin, A.M. Al-Alwani Mahmoud, A. Bakar Mohamad, A.A.H. Kadhum, K. Sopian, N.S. Abdul Karim, Renewable and Sustainable Energy Reviews, 31 (2014) 386-396.

[3] J.-F. Yin, M. Velayudham, D. Bhattacharya, H.-C. Lin, K.-L. Lu, Coordination Chemistry Reviews, 256 (2012) 3008-3035.

[4] N.S. Lewis, Science, 315 (2007) 798-801.

[5] J. Werner, Second and Third Generation Photovoltaics — Dreams and Reality, in: B. Kramer (Ed.) Advances in Solid State Physics, Springer Berlin Heidelberg, 2004, pp. 51-68.

[6] D.S. Kim, A.M. Gabor, V. Yelunder, A.D. Upadhyaya, V. Meemongkolkiat, A. Rohatgi, Photovoltaic Energy Conversion, 2003. Proceedings of 3rd World Conference on, 2003, pp. 1293-1296 Vol.1292.

[7] M. Späth, P.M. Sommeling, J.A.M. van Roosmalen, H.J.P. Smit, N.P.G. van der Burg, D.R. Mahieu, N.J. Bakker, J.M. Kroon, Progress in Photovoltaics: Research and Applications, 11 (2003) 207-220.

[8] R.M. Abbas Belfar, Journal of Applied Sciences, 11 (2011) 2932-2939.

[9] H.K. Jun, M.A. Careem, A.K. Arof, Renewable and Sustainable Energy Reviews, 22 (2013) 148-167.

[10] M.A. Green, K. Emery, Y. Hishikawa, W. Warta, E.D.Dunlop, Progress in Photovoltaics: Research and Applications, 21 (2013) 1-11.

[11] B. O'Regan, M. Gratzel, Nature, 353 (1991) 737-740.

[12] S. Rühle, M. Shalom, A. Zaban, Chemphyschem, 11 (2010) 2290-2304.

[13] E.H. Sargent, Nat Photon, 6 (2012) 133-135.

[14] O. Inganas, Nat Photon, 5 (2011) 201-202.

[15] M.A. Green, Springer-Verlag, (2006).

[16] M.M. Byranvand, K. Ali Nemati, B. Mohammad Hossein, Nano-Micro Letters, 4 (2012) 253-266.

[17] S. Mathew, A. Yella, P. Gao, R. Humphry-Baker, F.E. CurchodBasile, N. Ashari-Astani, I. Tavernelli, U. Rothlisberger, K. NazeeruddinMd, M. Grätzel, Nat Chem, 6 (2014) 242-247.

[18] T.N. Murakami, M. Grätzel, Inorganica Chimica Acta, 361 (2008) 572-580.

[19] W. Kwon, J.M. Kim, S.W. Rhee, Journal of Materials Chemistry A, 1 (2013) 3202-3215.

[20] G. Smestad, C. Bignozzi, R. Argazzi, Solar Energy Materials and Solar Cells, 32 (1994) 259-272.

[21] W.J. Lee, E. Ramasamy, D.Y. Lee, J.S. Song, ACS Applied Materials and Interfaces, 1 (2009) 1145-1149.

[22] W.-F. Chen, J.T. Muckerman, E. Fujita, Chemical Communications, 49 (2013) 8896-8909.

[23] Y. Xiao, J. Wu, J.-Y. Lin, S.-Y. Tai, G. Yue, Journal of Materials Chemistry A, 1 (2013) 1289-1295.

[24] X.H. Yang, J.W. Guo, S. Yang, Y. Hou, B. Zhang, H.G. Yang, Journal of Materials Chemistry A, 2 (2014) 614-619.

[25] L.-L. Li, E.W.-G. Diau, Chemical Society Reviews, 42 (2013) 291-304.

[26] T. Le Bahers, T. Pauporté, P.P. Lainé, F. Labat, C. Adamo, I. Ciofini, The Journal of Physical Chemistry Letters, 4 (2013) 1044-1050.

[27] D. Friedrich, L. Valldecabres, M. Kunst, T. Moehl, S.M. Zakeeruddin, M. Grätzel, Journal of Physical Chemistry C, 118 (2014) 3420-3425.

[28] J. Maçaira, L. Andrade, A. Mendes, Renewable and Sustainable Energy Reviews, 27 (2013) 334-349.

[29] M. Wang, C. Gratzel, S.M. Zakeeruddin, M. Gratzel, Energy & Environmental Science, 5 (2012) 9394-9405.

[30] M.K. Nazeeruddin, S.M. Zakeeruddin, J.J. Lagref, P. Liska, P. Comte, C. Barolo, G. Viscardi, K. Schenk, M. Graetzel, Coordination Chemistry Reviews, 248 (2004) 1317-1328.

[31] M. Grätzel, Accounts of Chemical Research, 42 (2009) 1788-1798.

[32] M.H. Bazargan, M.M. Byranvand, A.N. Kharat, International Journal of Materials Research, 103 (2012) 347-351.

[33] M.M.b. M. H. bazargan, A. nemati kharat, L. fatholahi, Optoelectronics and advanced materials – rapid communications, 5 (2011) 360 - 362.

[34] J.J. Vilatela, D. Eder, ChemSusChem, 5 (2012) 456-478.

[35] M.Q. Zhao, Q. Zhang, J.Q. Huang, F. Wei, Advanced Functional Materials, 22 (2012) 675-694.

[36] A.K. Geim, K.S. Novoselov, Nat Mater, 6 (2007) 183-191.

[37] A. Ghosh, Y.H. Lee, ChemSusChem, 5 (2012) 480-499.

[38] Y. Liang, H. Wang, J. Zhou, Y. Li, J. Wang, T. Regier, H. Dai, J. Am. Chem. Soc., 134 (2012) 3517-3523.

[39] F.D.S. Marquis, JOM, 63 (2011) 48-53.

[40] S. Bensaid, G. Centi, E. Garrone, S. Perathoner, G. Saracco, ChemSusChem, 5 (2012) 500-521.

[41] D.S. Su, S. Perathoner, G. Centi, Chem. Rev., 113 (2013) 5782-5816.

[42] S. Iijima, Nature, 354 (1991) 56-58.

[43] M. Zhang, J. Li, Materials Today, 12 (2009) 12-18.

[44] P. Poudel, Q. Qiao, Nano Energy, 4 (2014) 157-175.

[45] M. Asgari, E. Lohrasbi, ISRN Electrochemistry, 2013 (2013) 7.

[46] A. Shaikjee, N.J. Coville, Journal of Advanced Research, 3 (2012) 195-223.

[47] D.A. Stout, T.J. Webster, Materials Today, 15 (2012) 312-318.

[48] X. Zhao, R. Liu, Environment International, 40 (2012) 244-255.

[49] R.M. Osmani, A.S. Kulkarni, N.H. Aloorkar, R.R. Bhosale, P.P. Ghodake, B.R. Harkare, International Journal of Pharmaceutical and Clinical Research, 6 (2014) 84-96.

[50] S. Hatori, R. Matsuzaki, A. Todoroki, Composites Science and Technology, 92 (2014) 9-15.

[51] D. Janas, A.C. Vilatela, K.K.K. Koziol, Carbon, 62 (2013) 438-446.

[52] P. Avouris, M. Freitag, V. Perebeinos, Nature Photonics, 2 (2008) 341-350.

[53] A. Malapanis, V. Perebeinos, D.P. Sinha, E. Comfort, J.U. Lee, Nano Letters, 13 (2013) 3531-3538.

[54] M. Freitag, J.C. Tsang, A. Bol, D. Yuan, J. Liu, P. Avouris, Nano Letters, 7 (2007) 2037-2042.

[55] J.U. Lee, P.J. Codella, M. Pietrzykowski, Applied Physics Letters, 90 (2007).

[56] M. Freitag, J.C. Tsang, A. Bol, P. Avouris, D. Yuan, J. Liu, Applied Physics Letters, 91 (2007).

[57] Y.L. Kim, H.Y. Jung, S. Park, B. Li, F. Liu, J. Hao, Y.K. Kwon, Y.J. Jung, S. Kar, Nature Photonics, (2014).

[58] J. Wei, J.L. Sun, J.L. Zhu, K. Wang, Z. Wang, J. Luo, D. Wu, A. Cao, Small, 2 (2006) 988-993.

[59] M.E. Itkis, F. Borondics, A. Yu, R.C. Haddon, Science, 312 (2006) 413-416.

[60] S.W. Lee, B.M. Gallant, H.R. Byon, P.T. Hammond, Y. Shao-Horn, Energy & Environmental Science, 4 (2011) 1972-1985.

[61] G. Centi, S. Perathoner, Catalysis Today, 150 (2010) 151-162.

[62] J.-P. Tessonnier, M. Becker, W. Xia, F. Girgsdies, R. Blume, L. Yao, D.S. Su, M. Muhler, R. Schlögl, ChemCatChem, 2 (2010) 1559-1561.

[63] S. Thomas, T.G. Deepak, G.S. Anjusree, T.A. Arun, S.V. Nair, A.S. Nair, Journal of Materials Chemistry A, 2 (2014) 4474-4490.

[64] M.H. Bazargan, M.M. Byranvand, A.N. Kharat, Chalcogenide Letters, 7 (2010) 515-519.

[65] G. Calogero, P. Calandra, A. Irrera, A. Sinopoli, I. Citro, G. Di Marco, Energy and Environmental Science, 4 (2011) 1838-1844.

[66] E. Olsen, G. Hagen, S. Eric Lindquist, Solar Energy Materials and Solar Cells, 63 (2000) 267-273.

[67] I. Ahmad, J.E. McCarthy, M. Bari, Y.K. Gun'ko, Solar Energy, 102 (2014) 152-161.

[68] B. He, Q. Tang, T. Liang, Q. Li, Journal of Materials Chemistry A, 2 (2014) 3119-3126.

[69] B. He, Q. Tang, J. Luo, Q. Li, X. Chen, H. Cai, Journal of Power Sources, 256 (2014) 170-177.

[70] J. Ma, L. Zhou, C. Li, J. Yang, T. Meng, H. Zhou, M. Yang, F. Yu, J. Chen, Journal of Power Sources, 247 (2014) 999-1004.

[71] M. Wang, Q. Tang, H. Chen, B. He, Electrochimica Acta, 125 (2014) 510-515.

[72] R.D. Costa, F. Lodermeyer, R. Casillas, D.M. Guldi, Energy and Environmental Science, 7 (2014) 1281-1296.

[73] J.W. Guo, B. Zhang, Y. Hou, S. Yang, X.H. Yang, H.G. Yang, Journal of Materials Chemistry A, 1 (2013) 1982-1986.

[74] X. Sun, T. Chen, Z. Yang, H. Peng, Accounts of Chemical Research, 46 (2013) 539-549.

[75] M.J. Uddin, B. Davies, T.J. Dickens, O.I. Okoli, Solar Energy Materials and Solar Cells, 115 (2013) 166-171.

[76] G. Calogero, P. Calandra, A. Sinopoli, P.G. Gucciardi, International Journal of Photoenergy, 2010 (2010).

[77] S. Ito, Y. Mikami, Pure Appl. Chem., 83 (2011) 2089-2106.

[78] K. Suzuki, M. Yamaguchi, M. Kumagai, S. Yanagida, Chemistry Letters, 32 (2003) 28-29.

[79] H. Zheng, C.Y. Neo, J. Ouyang, ACS Applied Materials and Interfaces, 5 (2013) 6657-6664.

[80] Z. Yang, T. Chen, R. He, H. Li, H. Lin, L. Li, G. Zou, Q. Jia, H. Peng, Polymer Chemistry, 4 (2013) 1680-1684.

[81] H.J. Shin, S.S. Jeon, S.S. Im, Synthetic Metals, 161 (2011) 1284-1288.

[82] S. Bhandari, M. Deepa, A.K. Srivastava, C. Lal, R. Kant, Macromolecular Rapid Communications, 29 (2008) 1959-1964.

[83] F. Meng, X. Zhang, G. Xu, Z. Yong, H. Chen, M. Chen, Q. Li, Y. Zhu, ACS Applied Materials and Interfaces, 3 (2011) 658-661.

[84] G. Guan, Z. Yang, L. Qiu, X. Sun, Z. Zhang, J. Ren, H. Peng, Journal of Materials Chemistry A, 1 (2013) 13268-13273.

[85] D.-J. Yun, H. Ra, S.-W. Rhee, Renewable Energy, 50 (2013) 692-700.

[86] C.-T. Liu, Y.-C. Wang, R.-X. Dong, C.-C. Wang, K.-C. Huang, R. Vittal, K.-C. Ho, J.-J. Lin, Journal of Materials Chemistry, 22 (2012) 25311-25315.

[87] K.-C. Huang, Y.-C. Wang, R.-X. Dong, W.-C. Tsai, K.-W. Tsai, C.-C. Wang, Y.-H. Chen, R. Vittal, J.-J. Lin, K.-C. Ho, Journal of Materials Chemistry, 20 (2010) 4067-4073.

[88] M. Wu, Q. Zhang, J. Xiao, C. Ma, X. Lin, C. Miao, Y. He, Y. Gao, A. Hagfeldt, T. Ma, Journal of Materials Chemistry, 21 (2011) 10761-10766.

[89] G.R. Li, J. Song, G.L. Pan, X.P. Gao, Energy and Environmental Science, 4 (2011) 1680-1683.

[90] M. Wang, A.M. Anghel, B. Marsan, N.L.C. Ha, N. Pootrakulchote, S.M. Zakeeruddin, M. Grätzel, J. Am. Chem. Soc., 131 (2009) 15976-15977.

[91] X. Xin, M. He, W. Han, J. Jung, Z. Lin, Angewandte Chemie International Edition, 50 (2011) 11739-11742.

[92] F. Gong, H. Wang, X. Xu, G. Zhou, Z.S. Wang, J. Am. Chem. Soc., 134 (2012) 10953-10958.

[93] M. Wu, X. Lin, A. Hagfeldt, T. Ma, Angewandte Chemie - International Edition, 50 (2011) 3520-3524.

[94] M. Wu, X. Lin, Y. Wang, L. Wang, W. Guo, D. Qi, X. Peng, A. Hagfeldt, M. Grätzel, T. Ma, J. Am. Chem. Soc., 134 (2012) 3419-3428.

[95] J.-Y. Lin, S.-Y. Tai, S.-W. Chou, The Journal of Physical Chemistry C, 118 (2013) 823-830.

[96] D. Noureldine, T. Shoker, M. Musameh, T.H. Ghaddar, Journal of Materials Chemistry, 22 (2012) 862-869.

[97] G. Yue, J. Wu, J.Y. Lin, Y. Xiao, S.Y. Tai, J. Lin, M. Huang, Z. Lan, Carbon, 55 (2013) 1-9.

[98] Y. Xiao, J. Wu, J. Lin, G. Yue, J. Lin, M. Huang, Y. Huang, Z. Lan, L. Fan, Journal of Materials Chemistry A, 1 (2013) 13885-13889.

AUTHOR (S) BIOSKETCHES

Malekshahi Byranvand, M., Ph.D., School of Chemistry, University College of Science, University of Tehran, Tehran, Iran., Email: *Mahdi.malekshahi@gmail.com*